Nanoscale

Enzyme Assembly on Nanoparticle Scaffolds Enhances Cofactor Recycling and Improves Coupled Reaction Kinetics

Journal:	*Nanoscale*
Manuscript ID	NR-ART-02-2023-000729.R1
Article Type:	Paper
Date Submitted by the Author:	03-May-2023

Complete List of Authors:	Breger, Joyce; US Naval Research Laboratory, Center for Bio/Molecular Science and Engineering, Code 6900 Goldman, Ellen; US Naval Research Laboratory, Center for Bio/Molecular Science and Engineering, Code 6900 Susumu, Kimihiro; US Naval Research Laboratory, Optical Sciences Division, Code 5600; Jacobs Corporation Oh, Eunkeu; US Naval Research Laboratory, Optical Sciences Division, Code 5600 Green, Christopher; US Naval Research Laboratory, Center for Bio/Molecular Science and Engineering, Code 6900 Hooe, Shelby; US Naval Research Laboratory, Center for Bio/Molecular Science and Engineering Thakur, Meghna; US Naval Research Laboratory, Center for Bio/Molecular Science and Engineering; George Mason University College of Science Medintz, Igor; US Naval Research Laboratory, Center for Bio/Molecular Science and Engineering, Code 6900 Ellis, Gregory; US Naval Research Laboratory, Center for Bio/Molecular Science and Engineering, Code 6900

Enzyme Assembly on Nanoparticle Scaffolds Enhances Cofactor Recycling and Improves Coupled Reaction Kinetics

Joyce C. Breger[1], Ellen R. Goldman[1], Kimihiro Susumu[2], Eunkeu Oh[2],

Christopher M. Green[1], Shelby L. Hooe[1,3], Meghna Thakur[1,4],

Igor L. Medintz[1], and Gregory A. Ellis[1]*

[1]Center for Bio/Molecular Science and Engineering Code 6900
[2]Optical Sciences Division Code 5600
U.S. Naval Research Laboratory
Washington, D.C., 20375, USA

[3]National Research Council
Washington, D.C., 20001, USA

[4]College of Science
George Mason University
Fairfax, Virginia, 22030 USA

*Email: Gregory.ellis@nrl.navy.mil

Keywords: Enzyme, catalysis, nanoparticle, quantum dot, substrate channeling, glucose dehydrogenase, cofactor recycling, NADH.

ORCID Numbers: C.M.G. 0000-0001-7848-7144
E.O. 0000-0003-1641-522X
E.R.G. 0000-0001-9533-7455
G.A.E. 0000-0001-5559-3809
I.L.M. 0000-0002-8902-4687
J.C.B. 0000-0003-4198-5080
K.S. 0000-0003-4389-2574
M.T.
S.L.H.

Abstract

Enzyme activity can be many times enhanced in configurations where they are displayed on a nanoparticle (NP) and this same format sometimes even provides access to channeling phenomena within multienzyme cascades. Here, we demonstrate that such enhancement phenomena can be expanded to enzymatic cofactor recycling along with the coupled enzymatic processes that they are associated with. We begin by showing that the efficiency of glucose driven reduction of nicotinamide adenine dinucleotide ($NAD^+ \rightarrow NADH$) by glucose dehydrogenase (GDH) is enhanced *ca*. 5-fold when the enzyme is displayed on nanocrystalline semiconductor quantum dots (QDs) which are utilized as prototypical NP materials in our experimental assays. Coupling this enzymatic step with NADH-dependent lactate dehydrogenase (LDH) conversion of lactate to pyruvate also increases the latter's rate by a similar amount when both enzymes were jointly incorporated into self-assembled QD-based nanoclusters. Detailed agarose gel mobility assays and transmission electron microscopy imaging studies confirm that both tetrameric enzymes assemble to and crosslink the QDs into structured nanoclusters *via* their multiple-pendant terminal $(His)_6$ sequences. Unexpectedly, control experiments utilizing blocking peptides to prevent enzyme-crosslinking of QDs resulted in even further enhancement of individual enzyme on-QD kinetic activity. This activity was also probed revealing that 200-fold excess peptide/QD addition enhanced individual GDH and LDH on-QD k_{cat} a further 2- and 1.5×, respectively, above that seen just by QD display to a maximum of ~10-fold GDH enhancement. The potential implications for how these enzyme kinetics-enhancing phenomena can be applied to single and multi-enzyme cascaded reactions in the context of cofactor recycling and cell-free synthetic biology are discussed.

Introduction

The burgeoning field of synthetic biology seeks to replace many classic wet chemistry industrial processes with greener, biologically-based reactions that are almost all catalyzed by enzymes.[1-3] There are currently two main approaches being implemented towards this goal, namely that of cell-based and cell-free synthetic biology. Cell-based technologies seek to engineer chassis organisms such as *E. coli* and other cell types to recombinantly host heterologous genes comprising a designer synthetic or catabolic pathway that produces a desired product in significant quantities from a common substrate.[4-6] Potentially limiting issues here include energy-intensive maintenance of the cultures, the need to import and export key chemicals/substrates/products across cellular membranes, competing metabolic pathways, and a general intolerance *via* cellular toxicity to any non-natural substrates and products.[7] Cell-free synthetic biology looks to mitigate these specific issues by utilizing cellular extracts or designer reconstituted versions thereof to perform the required reactions.[8-11] Interest is also growing in 'minimalist' versions of a cell-free synthetic format where reactions only contain the minimal number of components required for a given multistep enzymatic pathway; these typically consist of just the necessary enzymes, cofactors, and substrates.[12, 13] Potential liabilities associated with this latter approach center primarily on achieving suitable mass transport and reaction efficiency along with maintaining long-term enzymatic stability. It is here that nanoparticle (NP) display of enzymes has much to offer for achieving such minimalist cell-free synthetic biology.

A growing body of work has now shown that a considerable number of enzyme types display enhanced kinetic activity when assembled on the surface of different nanoparticle (NP) materials. These enhancements typically manifest as an increased catalytic rate along with increased enzyme efficiency and, in rarer cases, some improvement to enzyme affinity.[14-19] The current belief is that the unique nanoscale environment that surrounds a colloidal NP imparts a strong influence on this enhancement process. Recent studies have confirmed that colloidal NPs universally structure their surrounding environment and that this structure may extend in length to a distance that is larger than the NP's diameter.[20, 21] The physical manifestation of this structured environment is largely unknown but it is postulated to have ionic, pH, and density gradients, along with acting as a soft or somewhat confining boundary between the nanoscale confines of the NP and that of the surrounding bulk solution.[22] Factors such as the type of bioconjugation chemistry used to attach the enzyme to the NP along with controlling the orientation of the enzyme on the

NP also appear to be important. Having the enzymes controllably oriented on the NP with all their active sites clearly available to incoming substrate appears to be a further contributing factor towards accessing this enhancement.[15-19, 23] NP size directly influences the enhancement of displayed enzymes with smaller NPs generally manifesting higher degrees of enhancement.[24] Larger NPs with their lower surface-to-volume ratios are constrained by more of a localized flat surface and the formation of an increased stagnation layer around the displayed enzyme due to laminar flow and related processes. Further, larger and flatter surfaces can cause an enzyme to flatten out upon attachment and jeopardize enzyme activity, whereas denaturation can be mitigated by immobilization onto highly curved (*i.e.*, nano-structured) particles.[17, 25, 26] When multimeric enzymes are attached to multiple NPs or to a single NP by multiple points, this can also help stabilize the enzymes' tertiary structure. This was shown unequivocally when the tetrameric lactate dehydrogenase (LDH) enzyme was attached to semiconductor quantum dots (QDs) by its four pendant termini, which led to the formation of small cross-linked QD-enzyme nanoclusters. Interestingly, in some cases when multiple enzymes constituting a pathway are incorporated into such cross-linked NP clusters, they can access substrate/intermediary channeling phenomena and display dramatically improved rates of catalytic flux.[27-29] Such probabilistic channeling functions mechanistically by increasing the rate of intermediary transfer between proximal enzymes in a manner that effectively competes with the much faster rate of product diffusion away from the enzyme.[30-32] We recently demonstrated self-assembled QD-nanoclustered cascades capable of channeling from 4- up to 10 enzymatic steps. Utilizing oxidative glycolysis and select saccharification enzyme as a model system, self-assembled QD cascades capable of improving overall catalytic flux by orders of magnitude were demonstrated.[33]

Our focus in this study is on evaluating how NP display of an enzyme and its subsequent enhancement along with access to any potential channeling phenomena can improve cofactor recycling (or regeneration) and the coupled reaction(s) that such recycled cofactors may be incorporated into. For biosynthetic cascades utilizing cofactors (*e.g.*, the relatively expensive redox nicotinamide adenine dinucleotide cofactor(s) $NAD(P)^+ \leftrightarrows NAD(P)H$), cofactor recycling using cheaper substrates (*e.g.*, glucose) will be crucial for economic feasibility. For this study, we chose a prototypical cofactor recycling enzyme, glucose dehydrogenase (GDH), which oxidizes glucose to glucono-$_D$-lactone, while recycling NAD(P)H from $NAD(P)^+$.[34-36] We begin by showing that the efficiency of GDH reduction of $NAD^+ \rightarrow NADH$ can be enhanced *ca*. 5 fold when the

enzyme is displayed on QDs. We also confirm that the enhancement holds when utilizing nicotinamide adenine dinucleotide phosphate ($NADP^+$) as substrate. We then sought to examine this in a coupled reaction utilizing cofactor recycling; we chose lactate dehydrogenase (LDH) as a model due to its well-studied nature and our previous examination of it immobilized onto QDs.[27, 33]

Coupling GDH regeneration of NADH to LDH conversion of pyruvate to lactate, which requires NADH, also increases the latter's rate by a similar amount when both enzymes are jointly incorporated into self-assembled QD-based nanoclusters, see schematic and reactions in **Figure 1A, B**. Detailed physicochemical analysis utilizing agarose gel mobility assays and transmission electron microscopy (TEM) imaging confirm that both these tetrameric enzymes assemble to and crosslink the QDs into structured nanoclusters. In control experiments aimed at assembly of separate QD-enzyme clusters, we unexpectedly found that addition of blocking peptides to individual QD-enzyme assemblies resulted in even further enhancement of individual enzyme on-QD kinetic activity. This led to GDH enhancements approaching 10× when incorporated into QD clusters. How such phenomena can be expanded into cell-free synthetic biology and contribute towards the development of this field is discussed.

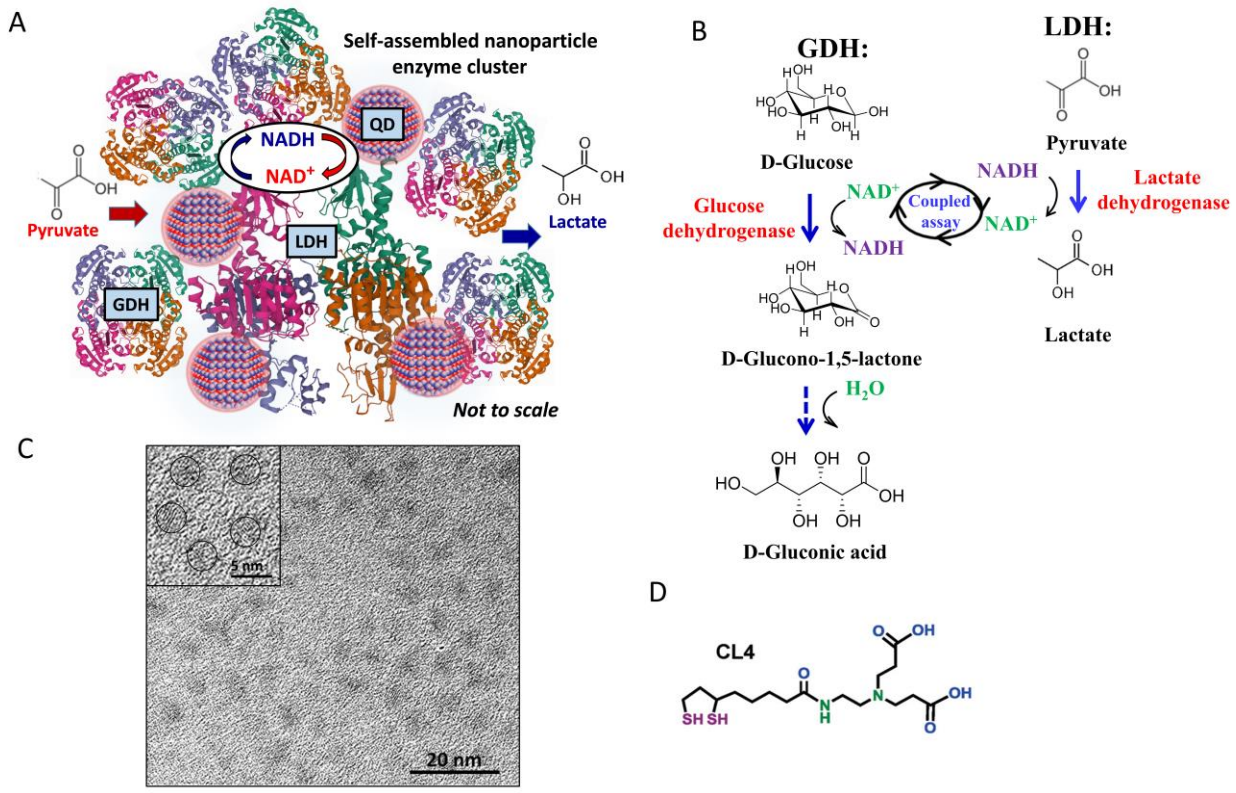

Figure 1. Self-assembled nanoparticle enzyme clusters and coupled catalysis. (A) Schematic of the nanoparticle-enzyme clusters that self-assemble. As shown, LDH (PDB # 3wx0) is the central enzyme with QDs attached at its 4 pendant $(His)_6$ termini. [37-41] When GDH is added, it also binds to the QDs. LDH and GDH (PDB # 3ay7) are able to both individually and jointly crosslink the QDs into nanoaggregated clusters.[37, 38, 41-43] When pyruvate is added to nanoclusters formed with both enzymes, this substrate is processed into lactate while the GDH recycles the cofactor NADH from NAD^+. GDH activity is enhanced when attached to QDs (both for forming NADH or NADPH), as is that of the coupled LDH-GDH reactions. The red halo around each of the QDs represents the presence of the CL4 ligand. **(B)** Coupled GDH-LDH reactions where GDH recycles NAD^+ to NADH using glucose as a substrate while LDH converts lactate to pyruvate with NADH as cofactor. (**C**) Representative TEM micrograph of the 523 nm emitting CdSe/CdS/ZnS core/shell/shell QDs with a diameter of 4.3 ± 0.5 nm. Inset shows a high-resolution image of several outlined QDs where crystal lattice structure is apparent. (**D**) Structure of the compact ligand CL4 with the thiols in the open dithiolane configuration.[44]

Results and Discussion

Enzymes, substrates, quantum dots, and nanocluster formation. A detailed description of all the materials and experimental formats along with the analyses utilized in this study can be found in the **Materials and Methods** section along with the accompanying **Supplementary Information** (**SI**). The *Bacillus megaterium* GDH gene was assembled, subcloned, and expressed

as described in the **Materials** section. This tetrameric enzyme is composed of 4 identical subunits, each with a mass of *ca*. 28 kDa. As shown in **Figure 1B**, GDH catalyzes the oxidation of D-glucose to glucono-$_D$-lactone; the lactone is subsequently hydrolyzed to D-gluconate in a non-enzymatic step in water. GDH catalyzes this reaction in a manner that is dependent on utilizing either NAD^+ or $NADP^+$ as cofactor which generates the corresponding reduced product.[43, 45-48] *E. coli*-derived lactate dehydrogenase (LDH) is also a homotetrameric enzyme whose 38.7 kDa subunits give rise to the ~154 kDa holoenzyme. LDH was prepared as described in detail in ref.[27] As a part of downstream glycolysis, LDH converts pyruvate to lactate using a reduced hydride donor/cofactor which produces the corresponding oxidized product. LDH can similarly use either NADH or NADPH as cofactor *albeit* with different affinity, efficiency, and preference depending upon which LDH enzyme variant is used.[49]

As the prototypical NP material for this study, we utilize 523 nm emitting CdSe/CdS/ZnS core/shell/shell QDs with a diameter of 4.3 ± 0.5 nm as determined by TEM, see **Figure 1C**.[50] To make the QDs colloidally stable in aqueous buffers, the QDs' native hydrophobic surface ligands were cap-exchanged with the CL4 ligand (**Figure 1D**).[44] This zwitterionic ligand has been repeatedly shown to provide QDs that are stable across a wide range of pH and ionic concentrations along with enabling biosensing and imaging applications in many challenging *in vitro* and *in vivo* environments.[51, 52] Critical to the current study, the small size of this ligand (<2 nm in length) allows for $(His)_n$-displaying proteins, peptides, and even appropriately-modified nucleic acids to coordinate to the QDs' ZnS outer shell *via* metal-affinity coordination.[53] $(His)_6$-motifs are typically appended to the termini of recombinantly expressed proteins for subsequent purification over Ni^{2+}-nitrilotriacetic acid (NTA) or similarly functionalized capture media.[54] As long as the $(His)_6$-motifs are clearly available on a given protein's surface, and not sterically precluded or hindered, the protein will coordinate to the ZnS-QDs in a nearly spontaneous manner where packing and protein display around the QD is dictated by an assembly process that follows a Poisson distribution and geometric fitting constraints.[55] For the specific instances where the proteins are multimeric (*e.g.*, dimers or tetramers) and display multiple pendant $(His)_6$ at their termini, it has been repeatedly confirmed that the QDs and enzymes, whether present individually or as part of a multienzyme cascade, will crosslink into nanoclusters by what appears to be a classical diffusion-limited aggregation (DLA) process.[27-29, 33, 56] This process also inherently dictates that the final size and structure of the resultant nanoclusters will depend on a complex interplay of the QD and enzyme(s)

concentrations present along with their size and shape and the reaction volume amongst other variables. This complex multivariable dependency means that, although the nanoclusters will form, their final size and shape cannot be predicted or controlled.

We began by confirming that the GDH did indeed self-assemble to the QD materials utilized here by undertaking agarose gel electrophoresis mobility shift assays (EMSAs). As shown in **Figure 2A** left set of images, equal amounts of QD were assembled with increasing ratios of GDH ranging from 0.5 up to 4 per QD and then loaded and separated in a 2% agarose gel under 1× TBE buffer. The evolution of migration shown in the image series reveals the formation of a higher molecular weight (MW) QD-GDH species with a slower rate of migration in the gel and the intensity of this slower species increases in a manner proportional to the amount of enzyme present. After 20 mins of separation, the samples corresponding to ratios of 2 through 4 GDH per QD show formation of a clearly distinct higher MW band above that of QD alone. Although clearly confirming that GDH does assemble to the QDs, the resolution of this assay format does not allow us to ascertain if this higher MW band reflects the presence of a singular or 1:1 QD:GDH conjugate, a higher valence species, or even a mix of QD species with different display ratios. Moreover, the sieving and separating nature of the EMSA may disrupt lower affinity or more-loosely bound QD-GDH conjugates. LDH assembly to ZnS overcoated QD materials stabilized with CL4 ligands has been shown previously and was again confirmed here in the same manner as GDH, see **Figure 2A** right set of images.[57] The ability of both LDH and GDH to simultaneously bind to QDs was next examined using the same EMSA format. **Figure 2B** highlights results where QDs were assembled with the indicated ratios of either no enzyme, each enzyme alone, or select ratios of both enzymes. When the QDs were assembled with a ratio of 2 of each enzyme, the mobility of the double conjugate is clearly different and of a higher MW than that of the individual QD-conjugate species assembled with just each enzyme alone at the same ratio (see left side of the gel images in **Figure 2B**). Similarly, the right side of the gel images show that changing the assembly ratio from 4 to 3 of each enzyme per QD also alters the mobility of the doubly-conjugated higher MW species. The same caveats as above about defining the exact nature and configuration of the higher MW species apply to these assemblies. Nevertheless, these results still confirm that both enzymes simultaneously bind to the QDs present in that reaction and that the conjugates that form also do this in a somewhat ratiometric-dependent manner.

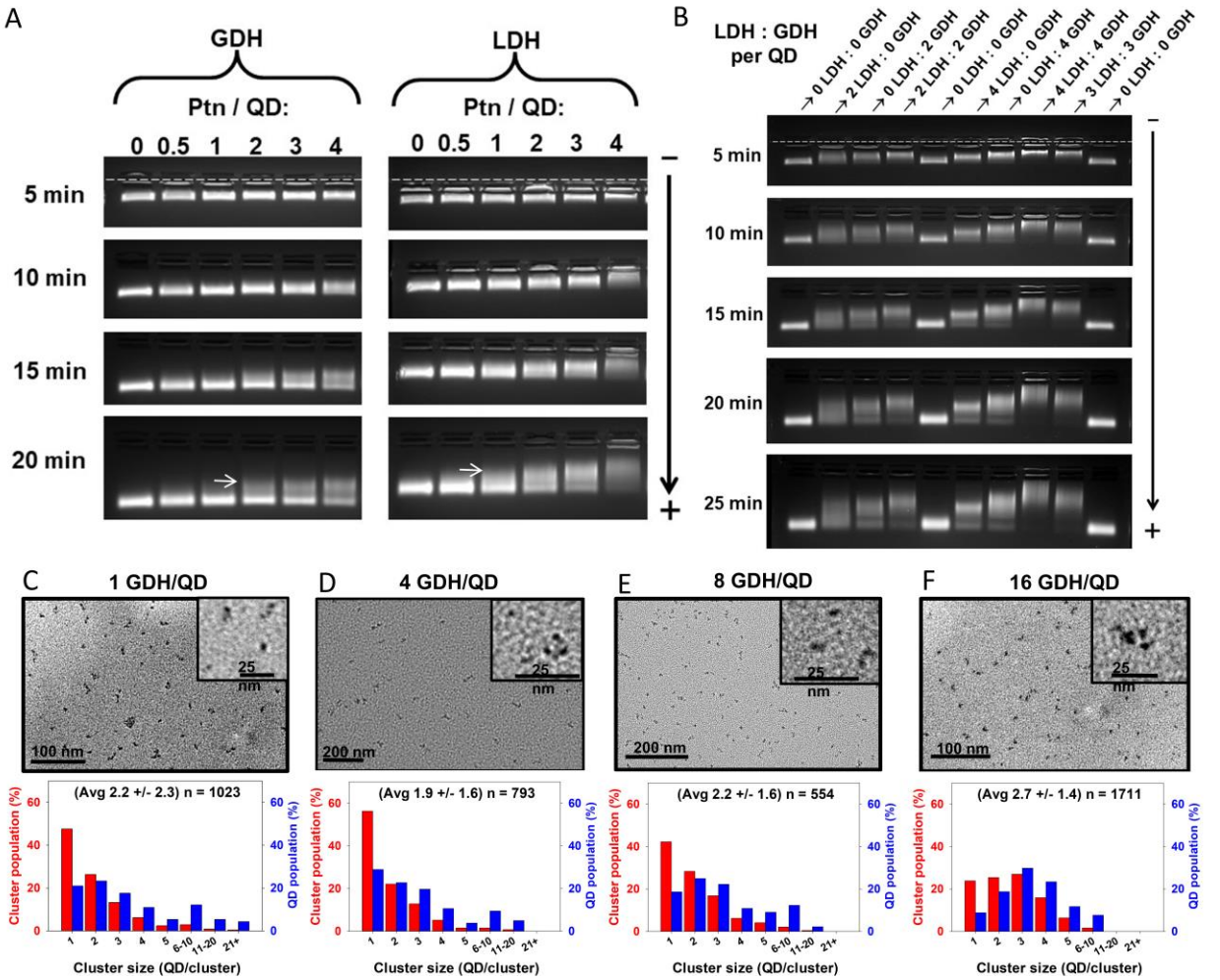

Figure 2. Agarose gel electrophoresis mobility shift assays and TEM analysis of QD-GDH aggregate formation. (A) QDs assembled with the indicated increasing ratios of GDH (left) or LDH (right) and then separated in 2% agarose gels run in 1×TBE buffer. Each lane contains 5 pmol of the 523 nm emitting QDs. Samples were separated using *ca*. 10 V per cm gel length and the runs stopped every 5 mins to collect an image. The location of the wells are indicated with the white dashed line in the top image. **(B)** QDs self-assembled with the indicated different ratios of LDH and GDH mixtures (LDH:GDH per QD) and then separated in 2% agarose gels run in 1×TBE buffer. Each lane contains 5 picoMoles of QD. Samples were separated using *ca*. 10 V per cm gel length and the runs stopped every 5 mins to collect images. The location of the wells in the gel are indicated with the white dashed line in the top image and white arrows indicate the slower mobility band. Representative TEM micrographs of 523 QDs assembled with a ratio of 1 **(C)**, 4 **(D)**, 8 **(E)**, and 16 **(F)**, GDH proteins per QD. Inset in each shows a high-resolution image of a cluster. In interpreting these images, it should be remembered that changes may have occurred either in deposition on the TEM grids or in the high vacuum of the TEM. Corresponding bar plots for each sample in (C-F) showing the distribution of cluster sizes present or cluster population (red) and number of QDs per cluster size (blue) as a percent. Average cluster size is given with each plot along with the number of QDs counted for that sample. The latter counting was performed manually by eye over several micrographs collected from imaging several assembled samples.

We next focused on confirming that the GDH tetramer could indeed crosslink with the QDs and form nanoaggregates in a manner similar to that noted previously with several other multimeric enzymes.[27, 29, 33] Using TEM for visualization and an analytical format that we had implemented previously,[33] the presence of QD aggregates forming was confirmed as shown by the representative TEM micrographs in **Figure 2C-F**. As noted repeatedly,[27, 29, 33] QD samples lacking GDH present were quite monodisperse in comparison, see **Supplementary Figure S1**. Interestingly, although all GDH ratios utilized drove QD-GDH nanoaggregate formation, the pattern of cluster sizes was not dramatically different for ratios ranging from 1 up to 8 GDH per QD with most clusters being of a smaller size, see the distributions of QD cluster sizes (red) and QD population percentage per cluster (blue) plotted below each representative TEM micrograph. The ratio of 16 seemed to change this with an increase in the percentage of QDs present in larger clusters. Although the TEM images were collected from material taken directly from assays (see below), we qualify the results as strictly semi-quantitative because of possible effects of TEM sample preparation and the limited number of samples examined. As mentioned above, this unpredictable assembly pattern most likely represents the complexity of the DLA formation process and the multiple factors that drive underlying cluster formation including QD size, protein shape, location of the QD-enzyme $(His)_6$-linkage point on the enzyme, relative concentrations, along with many others that are probably undefined. Indeed highlighting this point, performing a similar type of analysis with far larger 625 nm emitting QDs, which have a diameter of ~9.7 nm (**Supplementary Figure S1**), yielded different apparent cluster distributions with larger cluster sizes present for ratios ranging from 1 to 8 GDH per QD (**Supplementary Figure S2**). LDH ability to crosslink and form nanoclusters when self-assembling to CL4-displaying ZnS-overcoated QDs has been previously examined and confirmed.[27] Lastly, in a manner analogous to that shown in a previous report, we utilized polyacrylamide gel electrophoresis (PAGE) analysis to confirm the TEM results.[33] As shown in **Supplementary Figure S3**, addition of increasing QD to a constant concentration of GDH over a range of ratios from 25 GDH per QD down to 1 GDH per 5 QD depletes the native monomer band and results in the formation of a smear of higher molecular weight species. Moreover, this happens in a manner that changes visibly with the ratio of QD added. An almost identical result was obtained for PAGE analysis of LDH assembly to QDs as seen in **Supplementary Figure S4**. Cumulatively, the TEM and PAGE analysis provide

strong evidence that the GDH and LDH are capable of cross-linking the QDs into nanoaggregated structures in a somewhat ratio-dependent manner.

Glucose dehydrogenase enhancement when self-assembled with quantum dots into nanoclusters. Confident in the ability of the GDH to self-assemble to the QD surfaces and to form cross-linked nanoclusters with them, we next examined GDH kinetic activity in this configuration. For these assays, 5 nM GDH was assembled with an increasing ratio of QDs ranging from 1 up to 32 GDH per QD by keeping the enzyme concentration constant and varying the amount of QD added. Following assembly into nanoclusters, the individual samples were each assayed with increasing concentrations of glucose substrate in the presence of a fixed concentration of NAD^+ cofactor (1.46 mM). **Figure 3A** shows a representative set of progress curves monitoring NADH product formation as collected over time for these assemblies in 2.2 mM glucose. This setup was then applied for a range of glucose concentrations, the initial rates were estimated from fitting of the initial linear portion of each plot for the assembly ratios *versus* each glucose concentration, and then these were plotted using a standard Michaelis-Menten (MM) excess substrate format in **Figure 3B**; this analytical approach was utilized since the assay conditions met the classical Briggs-Haldane steady state conditions.[58] The corresponding kinetic descriptors derived from this data, including the maximum velocity (V_{Max}), catalytic rate (k_{cat}), the Michaelis constant (K_M) which reflects the enzyme's affinity for substrate, and k_{cat}/K_M a second order rate constant, which is used to describe enzyme efficiency are listed in the top of **Table 1**. The values presented here are all qualified as apparent since it is unclear if the QD-enzyme clusters strictly meet all of the MM assumptions; nevertheless, they still serve as an effective set of comparison metrics.

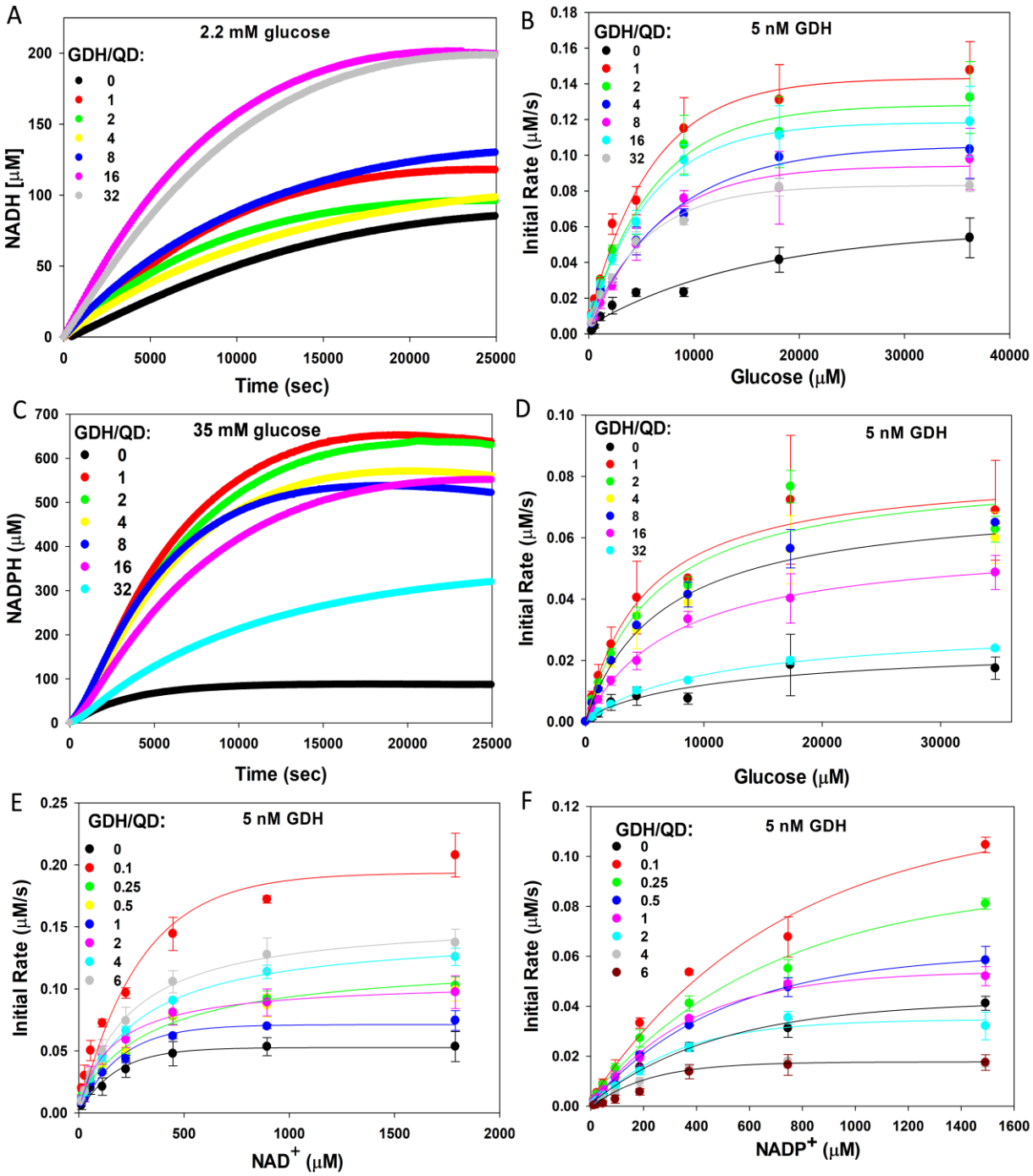

Figure 3. GDH kinetic assays. (A) Representative progress curve showing assay results where 5 nM GDH is assembled to the indicated increasing ratios of QDs and NADH conversion monitored over time in the presence of 2.2 mM glucose substrate. **(B)** Michaelis-Menten plot showing the initial rates of NADH conversion for 5 nM GDH assembled with the indicated increasing ratio of QDs *versus* increasing concentrations of glucose substrate. **(C)** Representative progress curve showing assay results where 5 nM GDH is assembled to the indicated increasing ratios of QDs and NADPH conversion monitored over time in the presence of 35 mM glucose

initial substrate. **(D)** Michaelis-Menten plot showing the initial rates of NADPH conversion for 5 nM GDH assembled with the indicated increasing ratio of QDs *versus* increasing concentrations of glucose substrate. **(E)** Michaelis-Menten plot showing the initial rates of NAD^+ conversion to NADH for 5 nM GDH assembled with the indicated ratios of QD in the presence of 16.6 mM glucose. **(F)** Michaelis-Menten plot showing the initial rates of $NADP^+$ conversion to NADPH for 5 nM GDH assembled with the indicated ratios of QD in the presence of 16.6 mM glucose.

In **Table 1** it is seen that k_{cat} increases almost 2.5× from ~14.1 to 34.9 turnovers per sec when comparing free GDH to that assembled at a 1-to-1 ratio of QD. k_{cat} then decreases in a somewhat linear fashion as a function of its increasing protein to QD ratio except for a small spike at a ratio of 16 GDH/QD. This generalized pattern of higher enhancement at lower ratios is similar to that seen with a variety of other enzymes when assembled with QDs in an analogous manner.[33, 59-62] Interestingly, the K_M values also decrease about 50% (*i.e*. better affinity) along with the increased k_{cat}, which is not something commonly seen with enzymatic enhancement on NP surfaces. Rather, the converse is normally seen where K_M typically increases as the catalytic rate improves.[59-62] Given this, the enzymatic efficiency (k_{cat}/K_M) is substantially enhanced above that of free enzyme (1.32 $mM^{-1} \times sec^{-1}$) ranging from *ca*. 3× for the ratio of 8 (4.05 $mM^{-1} \times sec^{-1}$) up to ~5.7× for the ratio of 1 (7.65 $mM^{-1} \times sec^{-1}$). As the ratio of GDH per QD changes from 1 up to 32, this clearly exerts an influence on enzyme kinetics. Separate from the phenomena that gives rise to the enzymatic enhancement when displayed on NPs, it still remains somewhat unclear if these changes in magnitude of kinetic enhancement with different ratios are also influenced by changes to enzyme crosslinking, enzyme stability, localized substrate sequestration or a complex combination of these and perhaps still other unknown factor(s) that characterize these self-assembled QD clusters.[14-19]

The same experiment as above was performed using identical QD-GDH assemblies but substituting in $NADP^+$ as the cofactor now. **Figure 3C** shows a representative set of progress curves monitoring NADPH formation over time for the assemblies in 35 mM glucose. Initial rates were estimated as above for each of the assembly ratios *versus* each glucose concentration and these are plotted in **Figure 3D**. The corresponding kinetic descriptors can be found listed in **SI Table S1** where a similar pattern of enhancement activity is seen. Note that by 25,000 sec there is a ~7× greater amount of NADPH for the best QD-GDH assembly over free GDH. The plots in **Figure 3E** and **3F** present assay data collected from QD-GDH assemblies, where assembly ratios

ranged from 1 up to 6, with glucose kept fixed in a large excess and the concentration of either NAD^+ or $NADP^+$ varied, respectively. Kinetic descriptors for these data are found in the middle and bottom of **Table 1**. For NAD^+ (**Figure 3E**), a similar pattern of enhancement is seen as for that of GDH *versus* glucose in **Figure 3B** with some notable differences. k_{cat} increases almost ~3× for a ratio of 0.1 GDH per QD (*i.e.* 10-fold excess QD) and the level of enhancement decreases linearly to the highest ratio of six where it is now only around 1.4-1.5× that of the free enzyme. In contrast to the above, the K_M values increases 2× (*i.e.* worse affinity) at the lowest ratio and then matches the native values within error for ratios of 0.25, 0.5, 1, 2 GDH per QD before increasing again for the two highest ratios of 4 and 6. The changes to k_{cat}/K_M here are almost completely in line with the changes to K_M because of the influence of the latter. Data from varying $NADP^+$, see **Figure 3F** and **Table 1**, show a similar pattern as that of NAD^+ assays except that values for k_{cat} are worse than free enzyme for the three highest ratios as are most of the K_M values except for the ratio of 4 GDH per QD which is almost half that of the free enzyme. This, in turn, means that enzyme efficiency for this cofactor when assembled in QD clusters increases at lower ratios and then drops below that of free enzyme at the highest ratios. Again, it appears that nanocluster properties have a complex influence on the underlying kinetic processes as the ratio of enzyme to QD changes. Since previous data indicated that some multimeric enzymes such as LDH can lose their tertiary structure and monomerize at low concentration with a subsequent loss of activity,[27] GDH activity was tested across a range of relevant concentrations, see **Supplementary Figure S5**. While inflection points in the graphs may show some subunit dissociation both free and on QDs, activity was still recorded over a range of dilute concentrations. This corresponds with studies that have shown reversible dissociation of the GDH tetramer by pH occurs in three steps: fast rearrangement with no activity loss, slow isomerization with lower specific activity, and then slow dissociation into inactive monomers.[63] Nicely, GDH enhancement by QDs was shown down to 1 nM GDH and up to 200 nM GDH (and by extrapolation, perhaps higher), indicating a broad range of GDH concentrations that could be enhanced by QDs.

Table 1. Estimated GDH Kinetic Parameters Measured On and Off QDs for Glucose, NAD^+, and $NADP^+$ as Substrates.

Ratio GDH per QD	V_{Max} (nM × sec^{-1})	k_{cat} (sec^{-1})	K_M (μM)	k_{cat}/K_M (mM^{-1} × sec^{-1})
Substrate: Glucose[a,b]				
0	66.8 ± 6.9	14.1 ± 1.5	10700 ± 2700	1.32 ± 0.36
1	165.9 ± 7.3	34.9 ± 1.5	4560 ± 630	7.7 ± 1.1
2	150.6 ± 8.3	31.7 ± 1.8	5140 ± 860	6.2 ± 1.1
4	123.9 ± 6.5	26.1 ± 1.4	6280 ± 940	4.15 ± 0.66
8	113.9 ± 7.5	24.0 ± 1.6	5900 ± 1100	4.05 ± 0.81
16	138.1 ± 6.5	29.1 ± 1.4	4750 ± 690	6.12 ± 0.93
32	95.3 ± 2.4	20.1 ± 0.5	4120 ± 340	4.86 ± 0.42
Substrate: NAD^{+}[a,c]				
0	50.3 ± 1.2	10.1 ± 0.2	157 ± 12	64.0 ± 5.0
0.1	155.3 ± 8.8	31.1 ± 1.8	350 ± 53	89 ± 14
0.25	102.0 ± 4.1	20.4 ± 0.8	158 ± 21	129 ± 18
0.5	86.1 ± 2.9	17.2 ± 0.6	188 ± 20	91 ± 10
1	81.4 ± 2.4	16.3 ± 0.5	133 ± 14	123 ± 13
2	69.9 ± 2.0	14.0 ± 0.4	168 ± 16	83.4 ± 8.1
4	70.9 ± 1.6	14.2 ± 0.3	214 ± 15	66.3 ± 4.9
6	74.7 ± 1.4	14.9 ± 0.3	231 ± 13	64.6 ± 3.8
Substrate: NADP^{+}[a,c]				
0	53.5 ± 2.1	10.7 ± 0.4	479 ± 45	22.3 ± 2.3
0.1	154.5 ± 9.6	30.9 ± 1.9	780 ± 99	39.6 ± 5.6
0.25	110.5 ± 5.7	22.1 ± 1.1	634 ± 68	34.8 ± 4.1
0.5	80.3 ± 3.1	16.1 ± 0.6	540 ± 48	29.7 ± 2.9
1	69.0 ± 3.1	13.8 ± 0.6	411 ± 47	33.6 ± 4.1
2	42.8 ± 3.1	8.6 ± 0.6	339 ± 65	25.3 ± 5.2
4	22.0 ± 1.4	4.4 ± 0.3	233 ± 41	18.9 ± 3.5
6	24.4 ± 3.0	4.9 ± 0.6	440 ± 130	11.1 ± 3.6

Notes: [a]GDH = 5 nM, [b]NAD^+=1,465 μM, [c]Glucose = 16.6 mM. Starting NAD^+= 1,578 μM. $NADP^+$ = 1,492 μM. Buffer = 100 mM phosphate pH 8. All kinetic values are qualified as apparent.

Coupled glucose dehydrogenase - lactate dehydrogenase activity when self-assembled with increasing ratios of quantum dots into nanoclusters. With a working understanding of how GDH would perform once assembled with QDs into nanoclusters, subsequent experiments focused on whether glucose-driven GDH turnover of NAD^+ to NADH could augment a coupled reaction. For this, the enzyme LDH was selected as it converts pyruvate to lactate with reduced NADH as the critical cofactor that is oxidized to NAD^+. Previous work assembling LDH into QD nanoclusters had shown that LDH activity was increased by >50-fold and its total turnover by >40-fold in this configuration; as mentioned previously, some of this improvement was ascribed to QD-

stabilization of the LDH tertiary structure.[27] More importantly when LDH and pyruvate kinase (PykA) were coassembled with QDs into nanoclusters, their colocalization led to >100-fold improvements in the rates of coupled activity with the bulk of the enhancement attributed to intermediary "channeling" between the QD-colocalized enzymes. LDH thus represented a well-characterized partner enzyme for preliminary testing of coupled activity with GDH.

As shown in **Figure 4A**, several different concentrations of GDH and LDH were tested in several parallel reactions with (5 and 20 nM QD added) or without undergoing coassembly with QDs (no QD control) (see also **Supplementary Figure S6, lanes 2–7**). To focus in on any specific role of channeling contributions to this coupled format, the amount of starting NAD^+ in the reaction was kept quite limiting at 123.1 μM *versus* 10 mM each glucose and pyruvate. As described in the **Methods** section, replicates from the parallel reactions were collected at select time points and subjected to LC-MS analysis to monitor lactate formation. When equimolar 2.5 nM concentrations of GDH and LDH were tested, a significant increase in lactate conversion of about 2.5× can be seen for the samples containing the highest 20 nM concentrations of QDs at the last 193 hr time point (1900 μM lactate produced) as opposed to the no QD control (750 μM lactate). The 5 nM QD sample showed some initial increases in lactate production at earlier time points but no significant differences with the no QD control at the later time points, see **Figure 4A** first three columns. In a replicate set of samples where GDH was increased 4-fold to 10 nM but LDH and QD concentrations remained the same, the amount of lactate produced by the last time point increased to *ca*. 2,700-2,800 μM for both the 5 and 20 nM QD samples. This corresponded to around 4× that produced for the free enzyme samples, see **Figure 4A** middle three columns. Interestingly, for both the QD containing samples, most of the reaction appeared to be complete by the initial 72 hr time point (~75-85% of 193 hr time point). The presence of more GDH in these reactions could help cycle the cofactor to the needed NADH state in a far more rapid manner. Given that GDH's estimated K_M for NAD^+ is at or approaches 3.5× (range 133-350 μM depending upon QD ratio present, see **Table 1**) that of the ~100 μM concentration present, having more enzyme present could help with conversion. Such a high rate of initial flux through the coupled system at earlier time points is also consistent with the presence of channeling phenomena in the nanoclusters, since channeling should manifest more prominently during the initial lag phase of multistep reactions.[32] Samples with just LDH present did not show any significant improvements to lactate production above that of the free enzyme controls which also serves to support the notion

of channeling being present in the clusters with coassembled enzymes, see **Figure 4A** right 3 columns. Lastly, increased lactate production in QD clustered samples where GDH concentration was increased 4× similarly point to this enzyme and its recycling of NAD^+ to the NADH that LDH requires as one of the key factors that augmented the coupled reaction. Moreover, the fact that activity here did not increase as might be presumed to occur due to the previously reported LDH increases in activity when on QD (~50×) may reflect that cofactor concentration or its putative rate of regeneration or channeling is the limiting factor. Similar to an approach described in a previous report,[33] we also implemented Förster resonance energy transfer- (FRET) based analytical assays to confirm that each enzyme did indeed assemble into the clusters with the other enzyme as they formed after QD addition (**Supplementary Figures S7** and **S8**. These assays did confirm co-assembly while also again confirming that the average enzyme presence in each cluster differs from the assembly stoichiometry. It should be noted that the co-presence of multiple QD donors and dye-labeled acceptors in a nanoclustered structure complicate the interpretation of these results.

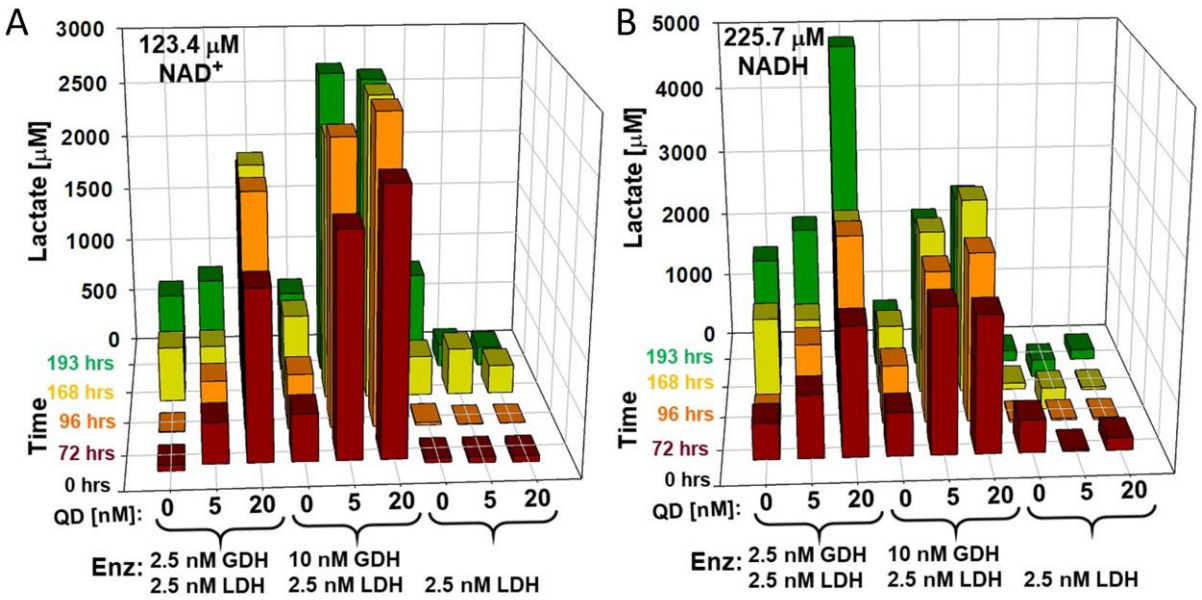

Figure 4. Coupled GDH-LDH assays and peptide blocking. Three-dimensional plots showing formation of lactate in reactions *versus* time where the indicated amounts of GDH and LDH were assembled with increasing amounts of QDs into nanoclusters or left free in solution. Reactions undertaken with either **(A)** 123.1 μM NAD^+ or **(B)** 225.7 μM NADH cofactor starting concentration. Samples were collected at the indicated time points from replicate assays and analyzed by LC-MS as described in the Methods to determine the lactate concentration. Within each plot, the ratios of GDH:LDH:QD used for each configuration going from left to right correspond to 1:1:0 (no QD control), 1:1:2, 1:1:8; 4:1:0 (no QD control), 4:1:2, 4:1:8, 0:1:0 (no QD control), 0:1:2, 0:1:8. All samples were run in triplicate and the results averaged. The standard deviation was found to be <5% of each value and are left out for simplicity.

Figure 4B presents representative results from the exact same configurations but using 225.7 μM NADH as the starting cofactor. Here a somewhat similarly-trending, but not identical, set of results are seen for lactate production. The difference in scale of lactate concentration between **Figure 4A** (3,000 μM) and **4B** (5,000 μM) shows that there is around 2.5× more production of lactate at the last 193 hr time point for the equimolar 2.5 nM GDH/LDH with and without QD as compared to using NAD^+ as a cofactor, see **Figure 4B** first 3 columns. The reason for this is not clear although a first thought is that having twice as much NADH present in the second configuration along with the fact that it does not need to be first reduced for LDH to use seems somewhat plausible. Previous assays estimated LDH's $K_{0.5}$ for NADH (concentration for half-maximal specific activity) when assembled to QDs as between 800-2,000 μM, thus having more cofactor present here may also helpful for coupled flux especially if there are any contributions from channeling-like phenomena.[27] However, lactate production for the samples with 4 times more GDH present are almost identical to that in panel **4A** within error arguing against this line of reasoning since this should only help with the rate of NAD^+ recycling, although it could affect the binding of LDH to QDs for its enhancement, see **Figure 4B** middle 3 columns. Overall, this illustrates the potential enhancements for these coupled, nanoscale systems while simultaneously highlighting inherent difficulties in defining all the responsible factors.

Effect of blocking peptide on enzyme activity within individual nanoclusters. In the previous study of PykA-LDH coupled activity when assembled to QDs, assembly of each enzyme to QDs as separate clusters prior to mixing significantly increased the lag time of the reaction suggesting that the intermediary pyruvate molecule was not as efficiently coupled between enzymes when they are not together in the same QD cluster; this served as one of several strong pieces of evidence

supporting channeling phenomena in that configuration.[27] Following on the results described above, a series of further experiments were undertaken to evaluate the contributions, if any, of channeling on the coupled GDH-LDH reactions. Since the channeling would be associated with formation of nanoclusters having both enzymes present in intimate proximity to each other, a series of side-by-side configurations where one or both enzymes are putatively excluded from the cluster but still remain free in solution were examined. To accomplish this, one enzyme was assembled to the QDs followed by sequential addition of an excess of blocking peptide for at least a one hour incubation period; this approach is based on using a methodology developed to keep $(His)_6$-appended enzymes from coassembling to similar QDs preloaded with substrate when that was not desired.[64] This allows each enzyme to bind to and cross-link with QDs into clusters with any remaining potential $(His)_6$ binding sites left available on the QDs in the cluster blocked by the added excess peptide. The other enzyme was then added to the sample before initiating the assay where the latter was meant to remain free in solution. In a derivative format, each enzyme is added to half the total amount of QD present in the assay followed by blocking peptide (both enzymes blocked) and then the two QD-enzyme samples added together. This latter format is meant to have each enzyme present in their own separate clusters within the same assay sample. The blocking peptide is added in ~200-fold excess concentration relative to each QD present. This concentration should effectively block any potential QD assembly site based on the 4.3 nm QD diameter in conjunction with the previously estimated upper limit of peptides that could assemble and fit around such a nanocrystal based on the $(His)_6$-binding footprint.[55] Similar samples were prepared by 'separate' assembly with no peptide blocker present as a control to evaluate any post-assembly interactions between each individual enzyme cluster.

Representative results from these experiments where the same enzyme ratios (10 nM GDH : 2.5 nM LDH, chosen from **Figure 4A**,**B**) were tested with QD at either 5 nM or 20 nM concentration are shown comparatively in **Figure 5A**,**B**, respectively. Assays were undertaken with 107.1 μM NADH cofactor starting concentration so as to allow some amount of direct incorporation by LDH in reactions rather than needing to be recycled first. The same trend in increase of lactate production between free GDH-LDH enzymes and those incorporated into QD clusters (no peptide blocker) as reported above in **Figure 4A,B** is again confirmed here, see **Figure 5A**,**B** first 2 columns. However, and quite unexpectedly, configurations where each enzyme was assembled to the QDs with peptide blocker while the other remained free (**Figure 5A**,**B** columns

3 and 4) or both were assembled in separate QD clusters with peptide blocker then mixed (**Figure 5A**,**B** column 5) showed significant increases in lactate production above that of both enzymes assembled into the same cluster (**Figure 5A**,**B** column 2). For the 10 nM GDH : 2.5 nM LDH: 5 nM QD samples in **Figure 5A**, the separated enzyme-cluster configurations reveal a *ca*. 1.5-2× increase in lactate production at the first 24 hr sampling point, which increases to ~3-3.5× at the last 148 hr sampling time point as compared to the original jointly-clustered non-blocked QD-enzyme assembly. These changes increase proportionally another ~3-3.5× fold if the comparison is made to the two enzymes when free in solution. The separately-assembled, not blocked ("separate") QD-GDH QD-LDH sample (**Figure 5A** column 5) shows a very slight 20% increase over the jointly-clustered QD-enzyme assembly except for the very last time point which is now at more than 2× increased lactate production.

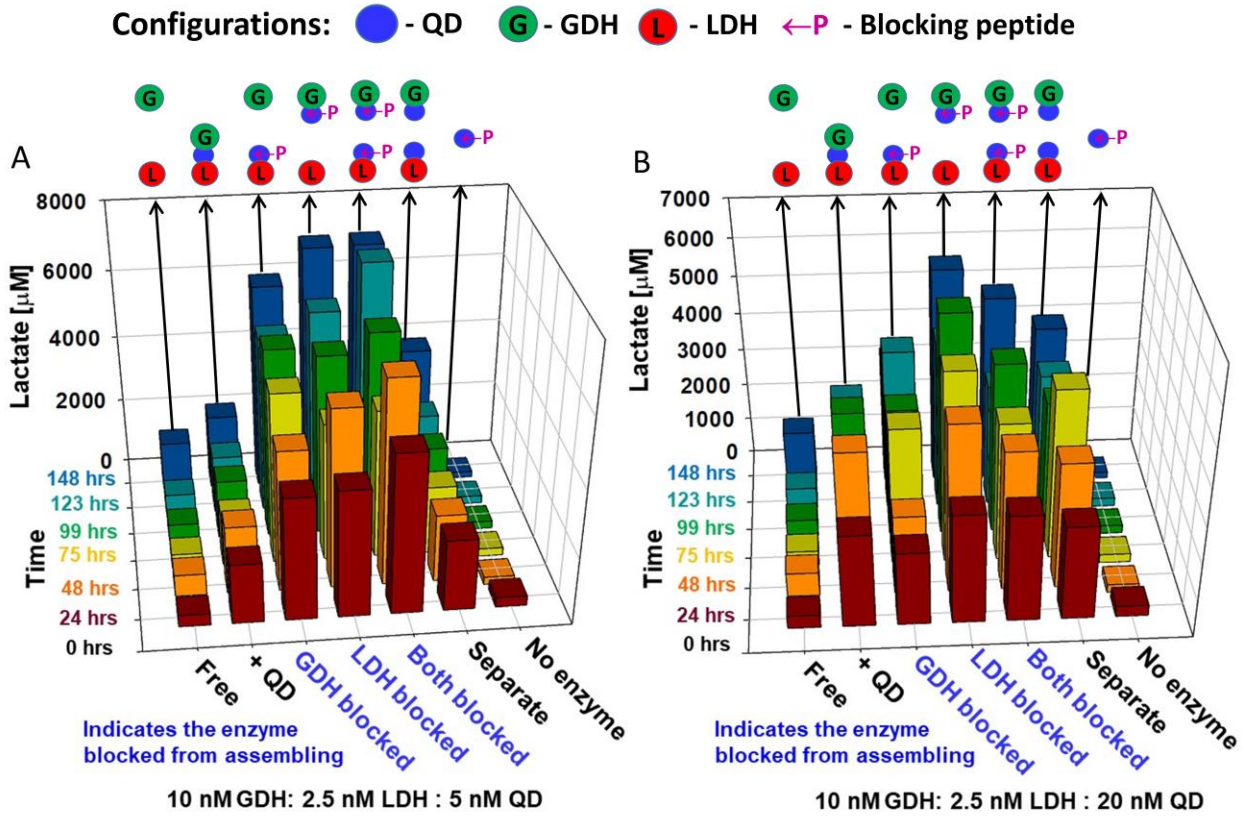

Figure 5. Coupled GDH-LDH assays with peptide blocking. (A) Three-dimensional plots showing formation of lactate in reactions *versus* time where 5 nM GDH and LDH were assembled in different configurations using peptide blocking with 5 nM QDs (ratio 4:1:2 GDH:LDH:QD) or left free in solution. **(B)** Results from identical assays where 20 nM GDH and LDH were assembled with 20 nM QDs (ratio 4:1:8) or left free in solution. Reactions were undertaken with 107.1 μM NADH cofactor starting concentration. Samples were collected at the indicated time points from replicate assays and analyzed by LC-MS to determine lactate concentration. Configurations tested include: free (no QD); +QD as in Figure 4A,B; LDH-QD with GDH blocked (LDH added to QDs, blocking peptide added next, then GDH free); GDH-QD with LDH blocked (GDH added to QDs, blocking peptide added next, then LDH free); both blocked (each enzyme added separately to 50% of total QD, blocking peptide added next, QD-enzymes mixed together), separate (each enzyme added separately to 50% of total QD, QD-enzymes mixed together, no blocking). Blue color indicates presence of blocking peptide in that QD-enzyme sample. All samples were run in triplicate and the results averaged. Standard deviation were <5% of each value and are left out for simplicity.

For the 10 nM GDH: 2.5 nM LDH: 20 nM QD samples in **Figure 5B**, the disparity between both enzymes assembled into the same cluster and the separated clusters is not as dramatic with only a few of the later time points for the GDH-QD with LDH blocked, separate blocked, and

separate not blocked samples showing significant increases over the jointly-clustered QD-enzyme assembly. Some of the samples here also produce more lactate at earlier time points as compared to the 5 nM samples, which is not unexpected given the 4× higher overall concentration of QD present which may induce larger cluster formation. Overall, this behavior is very different from that noted previously and represents our first observation of this particular phenomena, namely, increased kinetic activity that appears analogous to channeling when one or both enzymes are putatively assembled in their own QD cluster in the presence of a peptide blocker. This appears analogous to channeling in that kinetic activity is increased when coupling two enzymes, but disparate in that the two enzymes are presumably separated from each other. We also note that in this configuration the low overall amount of nicotinamide cofactor present may again function as a limiting factor despite the observed increases.

To provide insight into how underlying QD-enzyme cluster formation may influence these interesting results, we undertook both physicochemical and kinetic evaluations of the clusters formed for the LDH-QD with GDH blocked by peptide ("GDH blocked"), GDH-QD with LDH blocked ("LDH blocked"), each separate bound to QDs then blocked and mixed ("Both blocked"), and separate not blocked ("Separate") configurations. To confirm that each of the enzyme clusters were not cross-assembling with each other even when peptide-blocked, a two-color EMSA analysis was undertaken. To allow differentiation between each enzyme's specific QD cluster in this format, along with assembling LDH to the 523 nm emitting green QDs, we utilized 625 nm emitting red QDs, which were also surface functionalized with the zwitterionic CL4 ligand for assembly of the GDH. **Figure 6A** shows representative gel images collected from this analysis. The first four columns confirm the conjugation of LDH to green QDs (columns 1 and 2) and GDH to red QDs (columns 3 and 4). Both LDH and GDH attached to QDs then blocked (columns 9 and 10) show slower mobility then non-blocked versions (columns 2 and 4), perhaps indicating a more positive charge state or larger aggregates. Importantly, the different motilities for each color QD (columns 5-8) indicate that aggregates are not cross-assembling into higher-order structures (although for LDH on 523 QDs + peptide + 625-GDH this is less clear, column 5). We also note that GDH on 625 QDs + peptide do not enter the gel (columns 6, 7, and 10), and these samples even more clearly indicate no higher-order structures with LDH (columns 6 and 7). These compare with the 523-LDH and 625-GDH mixed without blocker (column 8) which demonstrates more color overlap and therefore higher-order structures with both LDH and GDH. Moreover, in the

mixed samples, the final mobility's match those seen for each individual sample separated by itself under the different assembly conditions. PAGE analysis of these samples helped confirm that GHD and LDH were being excluded from interacting with the QD-enzyme cluster when blocking peptide was added to the assembly reaction prior to their addition as intended in these formats, see **Supplementary Figure S6**.

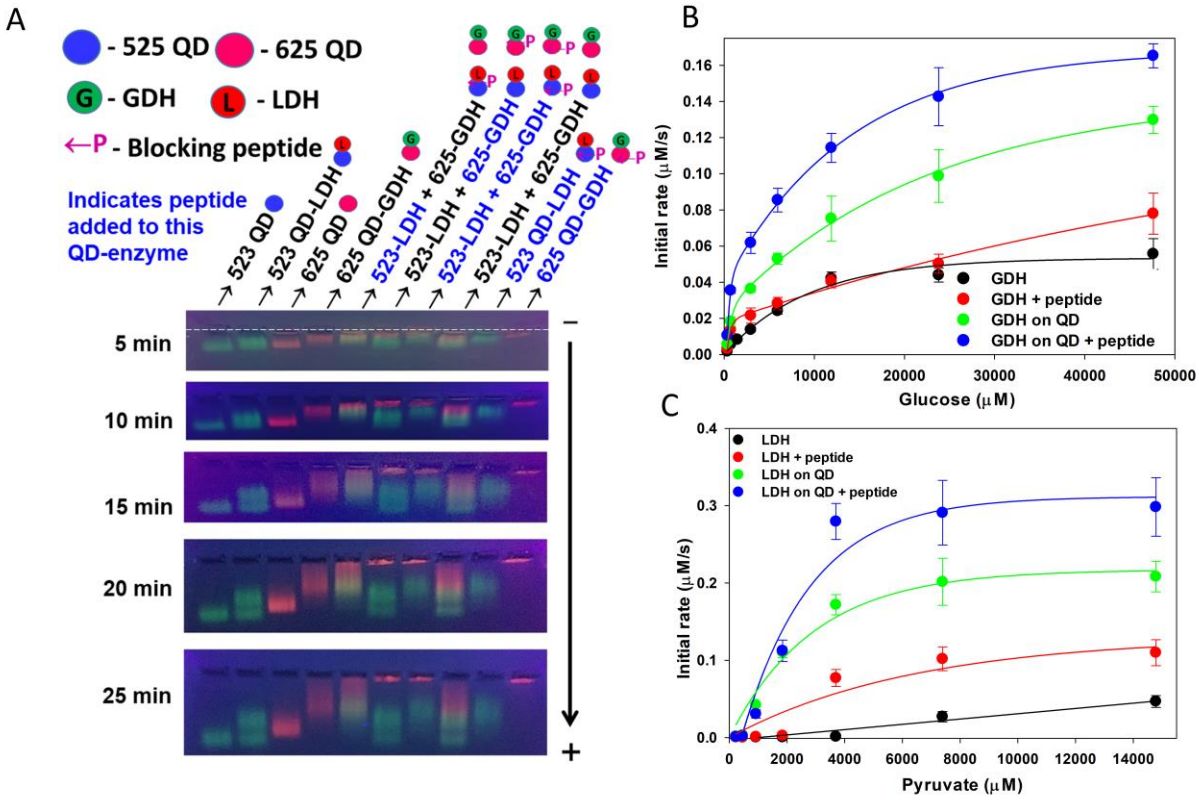

Figure 6. Probing of blocking peptide effects on individual QD-enzyme clusters. (A) 523 nm emitting QDs (green, 5 pmol) and 625 nm emitting QDs (red, 2 pmol) assembled with the indicated increasing ratios of LDH or GDH, respectively, along with blocking peptide where indicated and then separated in a 2% agarose gel run in 1×TBE buffer. Samples were separated using *ca.* 10 V per cm gel length and the run stopped every 5 mins to collect an image using a cellphone camera. Blue color indicates presence of blocking peptide in that QD-enzyme sample. The location of the wells are indicated by the white dashed line in the top image. Michaelis-Menten plots showing the initial rates of NADH conversion for **(B)** GDH or **(C)** LDH assembled as in Figure 5A,b with either peptide blocker, QDs, or both *versus* increasing concentrations of glucose or pyruvate substrate, respectively. Kinetic values and assay conditions are as listed in Table 2.

Continuing in the analysis of these constructs, **Figure 6B,C** shows MM plots collected from individual assays of similar concentrations of reactants as **Figure 4,5** of each enzyme free in solution, free enzyme with peptide, enzyme on QD (no peptide), and then enzyme on QD in the presence of peptide blocker. From just these assay results, it is clear that the presence of peptide with the QD-enzyme cluster can synergistically potentiate that enzyme's kinetic profile for GDH and LDH (compare green and blue lines). **Table 2** lists the kinetic values estimated from analyzing these data curves. Here, it is seen that just adding peptide to free GDH increases its k_{cat} >30% (see also **Figure 6B**, especially at low glucose concentrations). Similarly, adding peptide to QD-GDH clusters increases its k_{cat} by >15%. Adding peptide to QD-LDH clusters similarly increased its activity ~40%. In contrast, addition of peptide to free LDH decreased its activity ~20%, however, this calculated value may be skewed due to low LDH activity at low pyruvate concentrations, and the activity of LDH + peptide was seen to increase at higher pyruvate concentrations (**Figure 6C**). Testing QD-GDH clusters against increasing ratios of blocking peptide present did not reveal any specific trends in terms of ratio-dependent increases in initial rates (**Supplementary Figure S9**).

Determining the mechanism(s) behind how addition of peptide increases the catalytic rate of the already enhanced QD-enzyme clusters is beyond the current scope. Here, we just speculate on what some of the contributing factors may be. The prior experiments in other QD systems had utilized a blocking peptide that was negatively charged.[64] The blocking peptide utilized here (NH_2-GSWHHHHHH-amide) is relatively small with 9 residues and a MW of ~1171 g/mol. It is also relatively uncharged with a predicted value of *ca*. +1 at the pH of 7.5 used in the enzyme assays (determined using https://protcalc.sourceforge.net/). Nor is it very hydrophobic or hydrophilic *per se* although previous work with a similar neutral peptide seemed to cause some precipitation amongst larger diameter QDs.[64] What can be said with some certainty is that the peptide is jointly present in the QD-enzyme clusters. Both Wheeldon and Hess have presented almost unequivocal evidence supporting the concept that some types of enzyme clusters, and especially those that are DNA based where local charge state dominates, can interact with oppositely charged molecules, manifest localized substrate sequestration, which, in turn, enhances a given enzyme's catalytic activity.[65-71] Wheeldon has further suggested that, in many cases, these types of enhancements are often misinterpreted as channeling.[72] Supporting this latter notion, Klein utilized a 3-enzyme cascade assembled on a DNA triangle to show that although several of the enzymes manifest enhanced activity when assembled on the DNA scaffold, the enhancement of their joint flux was

just the additive sum of the individual enhancements and not a further non-linear contribution from channeling.[73] It is probable that a similar enhancement phenomena may be at work here to some extent. Another exciting possibility is that the joint QD-enzyme peptide system may be forming some type of peptide-driven coacervate; these are condensed liquid-like droplets formed by liquid–liquid phase separation of molecules through multiple weak associative interactions.[74, 75]

Table 2. Estimated GDH or LDH Kinetic Parameters Measured On and Off QDs in the Presence/Absence of Blocking Peptide with Glucose or Pyruvate Substrates.

Assembly conditions	V_{Max} (nM × sec^{-1})	k_{cat} (sec^{-1})	K_M (mM)	k_{cat}/K_M ($mM^{-1} \times sec^{-1}$)
Enzyme: GDH	**Substrate: Glucose**			
Free GDH[a]	66.2 ± 3.2	6.6 ± 0.3	9.5 ± 1.3	0.7 ± 0.1
GDH[a] + peptide[b]	90.8 ± 8.2	9.1 ± 0.8	13.5 ± 3.0	0.7 ± 0.2
GDH[a] on QD[c]	155.3 ± 8.1	15.5 ± 0.8	11.6 ± 1.6	1.3 ± 0.2
GDH[a] on QD[c] +peptide[b]	180.6 ± 6.2	18.1 ± 0.6	6.03 ± 0.68	3.0 ± 0.4
Enzyme: LDH	**Substrate: Pyruvate**			
Free LDH[d]	105.1 ± 27.2	42.0 ± 10.9	26.60 ± 11.47	1.6 ± 0.8
LDH[d] + peptide[e]	153.0 ± 17.8	30.6 ± 3.6	6.58 ± 2.08	4.7 ± 1.6
LDH[d] on QD[f]	231.9 ± 13.7	46.4 ± 2.7	2.30 ± 0.47	20.2 ± 4.3
LDH[d] on QD[f] + peptide[e]	329.1 ± 28.1	65.2 ± 5.6	2.53 ± 0.74	25.9 ± 7.9

Notes: [a]GDH = 10 nM, [b]Peptide = 1 μM, [c]QD = 5 nM, [d]LDH = 2.5 nM, [e]Peptide = 2 μM, [f]QD =1 0 nM, NAD^+=1,465 μM. Starting Glucose = 48 mM and NAD^+= 1,564 μM, pyruvate= 57 mM and NADH= 1,621 μM. Buffer = 100 mM phosphate pH 8. All kinetic values are qualified as apparent.

Conclusions

Overall, the results detailed above demonstrate significant activity enhancement to a cofactor recycling enzyme and that such enhancement can be coupled, in turn, to a cofactor utilizing enzyme. Unexpectedly but certainly fascinating, results of the peptide blocking experiments revealed another further mechanism to enhance enzyme activity within QD-enzyme clusters. Although not elucidated from a mechanistic perspective, the concept of a peptide-driven coacervate of some also suggests the exciting possibility of perhaps providing a means of controlling reaction rates in such NP-enzyme clusters by tailoring the peptide's chemical properties and thus its subsequent influence. Future experiments are in the planning stage to answer such questions. This study could not confirm the presence of channeling phenomena contributing to the enhanced activity of the coupled GDH-LDH system but cannot rule them out. The latter was

the primary focus of our previous work with PykA and LDH as assembled to QDs.[27] Despite this, at a minimum the results confirm that enzyme enhancement through assembly onto nanoparticles does have much to offer cell-free and especially minimalist multienzyme cascaded reactions. Indeed, a back of the envelope calculation suggests that the comparable cost of recycling an NADH or NADPH cofactor using glucose as the substrate versus that of purchasing the cofactor directly and adding it to the reactions is *ca*. $4x10^4 – 6x10^5$ fold less! (see the **SI**). Cumulative GDH activity enhancements from both QD display and then peptide presence approached >10× that of the free enzyme. As with the application of emergent phenomena to other more complex systems, it is probable that attempts to enhance other recycling enzymes and then applying that to a coupled enzyme system will need careful evaluation and testing since different configurations manifest different effects; compare for example, results for using NADH *versus* NADPH with GDH as the cofactor or adding peptide to LDH on QD (**Figure 3** and **4**). A continuing and confounding issue that remains largely unsolved here, and in general when working with similar material types, is that of characterizing the properties of the NP-enzyme and NP-enzyme-peptide bioconjugates. As mentioned, this arises as a result of the number of variables that influence the formation of these structures along with the lack of mature metrologies and techniques for analyzing these materials in intimate detail.[76]

Applications of cell-free multienzyme systems are expected to rapidly grow in the near future and many of these will be geared towards working with substrates, intermediaries, and final products that would typically be toxic to living chasses.[17, 18] This is because many enzymes can still act upon and modify substrates that would ultimately be toxic to a living cell. This will, in turn, allow such enzymatic systems to expand beyond natural products towards *de novo* and xenobiotic products.[77, 78] Due to intrinsic energy requirements, many, if not most of these types of systems will have reliance on cofactors as part of their cascaded steps and the ability to not only recycle the cofactors but also to either enhance the rate at which it happens or accomplish it with less material can be beneficial and help with cost effectiveness. Incorporating additional channeling phenomena into the mix within scaffolded enzyme-hosting architectures such as multienzyme clusters could potentially help further amplify such effects in a localized manner. We also acknowledge other various applications of GDH which may benefit from these results, including for biosensors and biofuel cells.[79-82] Future experimental efforts currently in planning will look toward testing channeling in other coupled-cofactor recycling enzyme systems in the

presence of more complex multienzyme cascades. Fully elucidating how cofactor recycling can not only be enhanced but also integrated into channeled multienzyme systems will ultimately allow this approach to be more widely adopted and utilized in a variety of cell-free biosynthetic applications.

Materials and Methods

Chemicals and Reagents. Nicotinamide adenine dinucleotide phosphate and related analogs (NAD^+, NADH, NADP, NADPH), IPTG, along with the other buffers, chemicals, and reagents used in this study were all sourced from Millipore Sigma or ThermoFisher Scientific. The blocking peptide NH_2-GSWHHHHHH-amide was obtained from Bio-Synthesis in the trifluoroacetic acid salt form and desalted as described.[83, 84] Phosphate buffer was 50 mM monophosphate and 50 mM diphosphate adjusted to pH 8 unless otherwise noted.

Quantum Dots. 523 nm emitting CdSe/CdS/ZnS core/shell/shell QDs were utilized as our experimental nanoparticulate material and these were synthesized as described previously.[44, 64, 85-89] The as-synthesized QDs stabilized with organic ligands were then cap-exchanged and made colloidally stable with the dihydrolipoic acid (DHLA)-appended compact ligand CL4 using a biphasic cap-exchange protocol as previously described.[44] 625 nm emitting QDs were prepared as described in refs.[24, 51, 61, 90, 91]

GDH Gene Construction, Protein Expression, and Purification. The gene for glucose dehydrogenase (GDH) from *Bacillus megaterium* (NCBI accession number BAA01476.1)[35, 47] was synthesized by GenScript. The construct was PCR amplified from the original vector to introduce Nde I and Xho I sites flaking the gene and cloned into the corresponding sites in the pET28b plasmid. The vector provides for an N-terminal hexahistidine or $(His)_6$ tag, but the PCR primer used to put in the cloning sites also introduced a stop codon before the Xho I site, preventing expression of the C-terminal histidine tail. All clones were verified by sequencing (Eurofins Genomics). Oligos were from Eurofins Genomics and cloning enzymes were purchased from New England Biolabs. Protein was produced using a protocol that had been previously described with only minor modifications.[92] Briefly, freshly transformed colonies of the *E. coli* Tuner (DE3) strain

were inoculated into 3 ml LB with kanamycin (kan, 30 μg/ml) and grown shaking at 37 °C overnight. The next day the entire overnight culture was used to inoculate 0.5 L of terrific broth (TB) kan and grown shaking at 37 °C for 6-7 hours. Then the temperature was lowered to 25 °C, and the cultures were induced with isopropyl-β-D-1 thiogalactoside (IPTG, 0.5 mM) and grown overnight. The following morning, cell pellets were suspended in ~30 mL phosphate-buffered saline (PBS) containing 0.05% Tween 20 and 1 mg of hen egg lysozyme was added to the cell suspension prior to sonication. After sonication, the cell debris was pelleted and supernatant incubated with immobilized metal affinity chromatography (IMAC) resin. Protein was eluted from the resin with 0.25 M imidazole solution. The final stage of purification was by fast protein liquid chromatography (FPLC) on an ENrich SEC 650 10 × 300 mm column (Bio-Rad). Protein concentration was determined using UV-visible spectroscopy and the molar extinction coefficient predicted from the protein sequence using the ExPASy online tool.[93] Protein yield was 42 mg/L. Following purification, the preparation was diluted to 50 μM in PBS with a final glycerol concentration of 20%. Protein was portioned into 50 μL aliquots, snap frozen on dry ice, and stored at -80 ^{o}C until use. LDH was prepared as previously described.[27]

Kinetic Assays. The kinetic assays were performed in a manner following the protocols described previously in Vranish *et al*.[27, 61, 83] Linear portions from the progress curves were used to calculate initial rates for each substrate concentration. These were then fitted with the Michaelis-Menten equation using Sigma Plot's enzyme module and the individual parameters derived.[62] Activity measurements were all performed on at least three replicates.

GDH Assays. The kinetic parameters for glucose dehydrogenase (GDH) were assessed in a similar manner as previously described in refs.[61, 83] Because GDH can utilize both NAD^+ and $NADP^+$ cofactors, the kinetic parameters for NAD^+, $NADP^+$, and glucose were assessed with the other assay constituents in vast excess. The final concentration of GDH was maintained at 5 nM while the final concentration of QD's ranged from 0 to 5 nM to achieve ratios of 0 to 32; higher protein to QD ratios are achieved by diluting the amount of QD present. Enzyme-QD bioconjugates were assembled in 100 mM phosphate buffer pH 8 at 4 ^{o}C then aliquoted to a 384-well plate. An equal amount of substrate solution was added to each well to start the reaction. When determining the kinetic parameters of GDH when NAD^+ or $NADP^+$ was held constant and

varying glucose, the substrate solutions consisted of 1.1 mM $NADP^+$ or 1.5 mM NAD^+ with the glucose ranging in final concentration from 0 to 33 mM. In the case of glucose being held constant and NAD^+ or $NADP^+$ varied, the substrate solution consisted of 30 mM glucose with either a range of 12 up to 1578 μM NAD^+ or 12 to 1492 μM $NADP^+$. The plate was then immediately placed in a Tecan Spark plate reader and the absorbance at 340 nm was measured over time for up to 16 hrs at 30 ^oC. The absorbance values were converted to concentration using the Beer-Lambert law and a molar extinction coefficient of 6220 M^{-1} cm^{-1}. The initial rates for each reaction was determined by calculating the slope of the linear portion of the progress curve. The initial rates were then fitted to the Michaelis-Menten (MM) equation by minimizing the error between the estimated initial rate and the measured initial rate to determine the apparent kinetic parameters in Sigma Plot.

Coupled LDH-GDH Enzyme Assays. To determine if GDH could facilitate greater lactate formation by LDH using pyruvate as a substrate, LDH was first assembled to increasing QD amounts to help stabilize and increase its activity as in ref.[27] followed by two different concentrations of GDH. As controls, equivalent amounts of LDH with or without GDH were not assembled to QDs. Specifically, QDs were aliquoted first to 1.5 mL tubes followed by LDH, allowed to assemble for 2 minutes, followed by the addition of GDH, and finally 50 mM phosphate buffer supplemented with 10 mM NaCl and 12 mM $MgCl_2$. The assemblies were allowed to incubate at 4 ^oC for at least 2 hrs to ensure complete assembly. 8-well PCR strips were used to house each of the different samples and their replicates so that at each time point an entire strip would be removed; this facilitated keeping all samples at each time point together and in the same order. To each 8-well PCR strip 100 μL of sample was added followed by 100 μL of substrate solution. These samples were then supplemented with 0, 5 nM, or 20 nM QDs. The substrate solution consisted of 123.1μM NAD^+ or 225.7 μM NADH, 10 mM glucose, and 10 mM pyruvate in 100 mM phosphate buffer pH 8 supplemented with 10 mM NaCl and 12 mM $MgCl_2$. The 8-well strips were placed in a PCR tube holder and placed in a table top shaking incubator set at 30 ^oC. Samples were collected as indicated and immediately placed in a -80 ^oC freezer to stop the reaction. Samples were thawed by placing them in a 90 ^oC heat block and to also ensure the reaction did not restart by denaturing the enzymes and then prepared for subsequent LC-MS analysis.

Peptide Blocking Assays. Eleven different samples were assembled. Enzyme concentration was kept constant with all samples having 2.5 nM LDH and 10 nM GDH. QD concentration was either 0, 5, or 20 nM while the blocking peptide was 200-fold greater than the QD concentration (1000 or 4000 nM). Samples were made in 100 mM phosphate buffer pH 8 with at least a 1 hour incubation time in between each addition to allow for assembly. In general, the order of addition was QD, LDH, ± peptide, GDH, and finally buffer. If LDH was to be blocked then the order was QD, GDH, ± peptide, LDH, and finally buffer. If each enzyme was to be assembled to their own QD then the order of assembly was QD, enzyme, ± peptide, and buffer followed by aliquots of each being mixed together prior to the start of the experiment. Samples were allowed to incubate for another two hours to allow for complete assembly. 100 μL aliquots were added to labeled tubes followed by 100 μL of substrate. Tubes were placed in an incubator at 30 ^{o}C with mild rotation. The substrate solution consisted of the following at final concentration: 107.1 μM NADH, 40.7 mM glucose, 40.8 mM pyruvate, 10 mM NaCl, and 12 mM $MgCl_2$. At each prescribed time point, a set of aliquots was pulled and quickly frozen at -80 ^{o}C. Samples were thawed at 90 ^{o}C prior to preparation for mass spectral analysis.

Mass Spectral Analysis of Lactate Formation from LDH-GDH Assays. LC-MS analyses were carried out on an Acquity H-Class UPLC equipped with a SQ2 MS detector based on a single quadrupole analyzer and an electrospray ionization source (Waters Corp, Milford, MA) as described previously.[29] Samples were separated on an Atlantis Premier BEH Z-HILIC, 2.1 x 100 mm, 1.7 um, column. A stock of 400 mM ammonium acetate was adjusted to pH 9 with ammonium hydroxide, and used for buffer construction. Buffer A was 10 mM ammonium acetate in H_2O. Buffer B was 10 mM ammonium acetate in 10:90 H_2O:acetonitrile. Flow rate was 0.25 mL/min and the column was held at a heated temperature 45 °C. Standards were first prepared by dilution into buffer. Samples and standards (49 μL) were then prepared for analysis by addition of the internal standard succinic acid-2,2,3,3-d4 (1 μL) followed by dilution into 50:50 methanol:acetonitrile (200 μL), centrifugation at 16,000 x g for 10 min, and transfer of the supernatant to analysis vials. Injection volume was 4 μL, and the acquisition gradient was as follows: initially hold at 90% B for 1.5 min, linear gradient from 90-60% B for 7 min, hold at 60% B for 4.5 min to wash, linear gradient from 60-90% B for 0.5 min, re-equilibrate by holding at 90% B for 7.5 min. Mass spectrometry was determined in-line with 3 kV capillary voltage in

negative mode. Selected ion recording (SIR) was done for selected components, including pyruvate, lactate, and the internal standard succinic acid-2,2,3,3-d4. ES negative scan was done between 20–3000 m/z. Mass spectral chromatograms were compared between reactions and standards, accounting for the internal standard.

Agarose Gel Electrophoresis. Low electroendosmosis (EEO) agarose gels formed in 1× TBE buffer (89 mM Tris, 89 mM boric acid, 2 mM EDTA pH 8.3) were utilized to confirm assembly of enzyme(s) to the CL4-functionalized QDs. Within each of the sample, 5 pmol of QD was allowed to self-assemble with the indicated molar ratio of enzyme for at least 1 h in 1 × PBS (137 mM NaCl, 2.7 mM KCl, 8 mM Na_2HPO_4, and 2 mM KH_2PO_4, pH 7.4). Samples consisting of a total 25 μL volume were then mixed with 5 μL gel loading buffer and then loaded into the individual wells of the gel placed under 1× TBE buffer in the gel box. The gel was run at ~10 V/cm length and images were captured every 5 min with a BioRad Molecular Imager ChemiDoc XRS+ system from the UV excited QD photoluminescence.

Transmission Electron Microscopy. Samples were prepared and TEM imaging of QDs and the QD-enzyme conjugates was performed using a Thermo Scientific Talos F200C G2 Cryo S/TEM, operated under standard TEM mode at 200 kV accelerating voltage in a manner similar to that described previously.[27, 50]

Conflicts of Interest. There are no conflicts to declare.

Acknowledgements. The authors acknowledge ONR, NRL, and the NRL Nanoscience Institute for funding support. S.L.H. acknowledges an NRC Fellowship through NRL. I.L.M. and G.A.E acknowledge the National Institute of Food and Agriculture, U.S. Department of Agriculture, under Award #2020-67021-31254, and the Strategic Environmental Research and Development Program (SERDP), under Award # WP21-1073 New Start Project (W74RDV03497375).

Supplementary Information. This includes further supporting data, images, and results and is available free of charge at the Journals website.

Author Contributions. J.C.B. and E.R.G. cloned and/or expressed the enzymes utilized in this study. K.S. prepared the QD materials along with synthesizing the CL4 ligand. J.C.B. and G.A.E. undertook the enzyme assays. E.O. and C.M.G. undertook the TEM experiments and subsequent analysis. J.C.B., G.A.E., S.L.H., M.T., and I.L.M. collected experimental data, analyzed samples,

and interpreted data. The manuscript was co-written by I.L.M. and G.A.E. with input from all authors. I.L.M. and G.A.E. procured project funding and provided research oversight. All authors have given approval to the final version.

References

1. National Research Council, *Industrialization of Biology: A Roadmap to Accelerate the Advanced Manufacturing of Chemicals*, The National Academies Press, Washington, DC, 2015.
2. A. Biz, S. Proulx, Z. Q. Xu, K. Siddartha, A. M. Indrayanti and R. Mahadevan, *Biotechnology Advances*, 2019, **37**, 107379.
3. J. M. Clomburg, A. M. Crumbley and R. Gonzalez, *Science*, 2017, **355**, aag0804.
4. J. D. Keasling, *Science*, 2010, **330**, 1355-1358.
5. S. Y. Lee and H. U. Kim, *Nature Biotechnology*, 2015, **33**, 1061-1072.
6. S. Y. Lee, H. U. Kim, T. U. Chae, J. S. Cho, J. W. Kim, J. H. Shin, D. I. Kim, Y.-S. Ko, W. D. Jang and Y.-S. Jang, *Nature Catalysis*, 2019, **2**, 18-33.
7. L. H. Jiang, J. R. Zhao, J. Z. Lian and Z. N. Xu, *Synthetic and Systems Biotechnology*, 2018, **3**, 90-96.
8. Y. Lu, *Synthetic and Systems Biotechnology*, 2017, **2**, 23-27.
9. C. Meyer, Y. Nakamura, B. J. Rasor, A. S. Karim, M. C. Jewett and C. M. Tan, *Life-Basel*, 2021, **11**, 551.
10. V. Noireaux and A. P. Liu, in *Annual Review of Biomedical Engineering, Vol 22*, ed. M. L. Yamush, 2020, vol. 22, pp. 51-77.
11. J. Garamella, R. Marshall, M. Rustad and V. Noireaux, *ACS Synthetic Biology*, 2016, **5**, 344-355.
12. J. U. Bowie, S. Sherkhanov, T. P. Korman, M. A. Valliere, P. H. Opgenorth and H. Liu, *Trends in Biotechnology*, 2020, **38**, 766-778.
13. K. S. Rabe, J. Muller, M. Skoupi and C. M. Niemeyer, *Angewandte Chemie-International Edition*, 2017, **56**, 13574-13589.
14. S. A. Ansari and Q. Husain, *Biotechnology Advances*, 2012, **30**, 512-523.
15. B. J. Johnson, W. Russ Algar, A. P. Malanoski, M. G. Ancona and I. L. Medintz, *Nano Today*, 2014, **9**, 102-131.
16. G. A. Ellis, S. N. Dean, S. A. Walper and I. L. Medintz, *Catalysts*, 2020, **10**, 83.
17. G. A. Ellis, S. A. Díaz and I. L. Medintz, *Current Opinion in Biotechnology*, 2021, **71**, 77-90.
18. G. A. Ellis, W. P. Klein, G. Lasarte-Aragonés, M. Thakur, S. A. Walper and I. L. Medintz, *ACS Catalysis*, 2019, **9**, 10812-10869.
19. J. N. Vranish, M. G. Ancona, S. A. Walper and I. L. Medintz, *Langmuir*, 2018, **34**, 2901-2925.
20. M. Zobel, R. B. Neder and S. A. J. Kimber, *Science*, 2015, **347**, 292-294.
21. S. L. J. Thoma, S. W. Krauss, M. Eckardt, P. Chater and M. Zobel, *Nature Communications*, 2019, **10**.

22. C. Pfeiffer, C. Rehbock, D. Huhn, C. Carrillo-Carrion, D. J. de Aberasturi, V. Merk, S. Barcikowski and W. J. Parak, *Journal of the Royal Society Interface*, 2014, **11**, 20130931.
23. I. Medintz, *Nature Materials*, 2006, **5**, 842-842.
24. J. C. Breger, E. Oh, K. Susumu, W. P. Klein, S. A. Walper, M. G. Ancona and I. L. Medintz, *Bioconjugate Chemistry*, 2019, **30**, 2060-2074.
25. A. A. Vertegel, R. W. Siegel and J. S. Dordick, *Langmuir*, 2004, **20**, 6800-6807.
26. Y. M. Wang, R. Jonkute, H. Lindmark, J. D. Keighron and A. S. Cans, *Langmuir*, 2020, **36**, 37-46.
27. J. N. Vranish, M. G. Ancona, E. Oh, K. Susumu, G. Lasarte Aragonés, J. C. Breger, S. A. Walper and I. L. Medintz, *ACS Nano*, 2018, **12**, 7911-7926.
28. M. Thakur, J. C. Breger, K. Susumu, E. Oh, J. R. Spangler, I. L. Medintz, S. A. Walper and G. A. Ellis, *PLoS ONE*, 2022, **17**, e0265274.
29. S. Hooe, J. Breger, S. Dean, K. Susumu, E. Oh, S. Walper, G. A. Ellis and I. L. Medintz, *ACS Applied Nano Materials*, 2022, **5**, 10900–10911.
30. M. Castellana, M. Z. Wilson, Y. Xu, P. Joshi, I. M. Cristea, J. D. Rabinowitz, Z. Gitai and N. S. Wingreen, *Nature Biotechnology*, 2014, **32**, 1011-1018.
31. H. O. Spivey and J. Ovadi, *Methods*, 1999, **19**, 306-321.
32. I. Wheeldon, S. D. Minteer, S. Banta, S. C. Barton, P. Atanassov and M. Sigman, *Nature Chemistry*, 2016, **8**, 299-309.
33. J. C. Breger, J. N. Vranish, E. Oh, M. H. Stewart, K. Susumu, G. Lasarte-Aragones, G. A. Ellis, S. A. Walper, S. A. Diaz, S. L. Hooe, W. P. Klein, M. Thakur, M. G. Ancona and I. L. Medintz, *Nature Communications*, 2023, **14**, 1757.
34. A. Basso, M. S. Brown, A. Cruz-Izquierdo, C. A. Martinez and S. Serban, *Organic Process Research & Development*, 2022, **26**, 2075-2084.
35. M. Dirkmann, J. Nowack and F. Schulz, *Chembiochem*, 2018, **19**, 2146-2151.
36. X. Wang, T. Saba, H. H. P. Yiu, R. F. Howe, J. A. Anderson and J. Shi, *Chem*, 2017, **2**, 621-654.
37. H. Berman, K. Henrick and H. Nakamura, *Nature Structural & Molecular Biology*, 2003, **10**, 980.
38. H. M. Berman, J. Westbrook, Z. Feng, G. Gilliland, T. N. Bhat, H. Weissig, I. N. Shindyalov and P. E. Bourne, *Nucleic Acids Research*, 2000, **28**, 235-242.
39. N. Furukawa, A. Miyanaga, M. Nakajima and H. Taguchi, *Biochemistry*, 2018, **57**, 5388-5406.
40. N. Furukawa, M. Togawa, A. Miyanaga, M. Nakajima and H. Taguchi, The crystal structure of D-lactate dehydrogenase from Escherichia coli, https://doi.org/10.2210/pdb3wx0.pdb).
41. D. Sehnal, S. Bittrich, M. Deshpande, R. Svobodova, K. Berka, V. Bazgier, S. Velankar, S. K. Burley, J. Koca and A. S. Rose, *Nucleic Acids Research*, 2021, **49**, W431-W437.
42. T. Nishioka, Y. Yasutake, Y. Nishiya and T. Tamura, Crystal structure of Bacillus megaterium glucose dehydrogenase 4 G259A mutant, https://doi.org/10.2210/pdb3ay7/pdb).
43. T. Nishioka, Y. Yasutake, Y. Nishiya and T. Tamura, *Febs Journal*, 2012, **279**, 3264-3275.
44. K. Susumu, E. Oh, J. B. Delehanty, J. B. Blanco-Canosa, B. J. Johnson, V. Jain, W. J. Hervey, W. R. Algar, K. Boeneman, P. E. Dawson and I. L. Medintz, *Journal of the American Chemical Society*, 2011, **133**, 9480-9496.

45. P. K. Srivastava and S. Singh, *Preparative Biochemistry & Biotechnology*, 2013, **43**, 376-384.
46. K. Stolarczyk, J. Rogalski and R. Bilewicz, *Bioelectrochemistry*, 2020, **135**, 107574.
47. T. Nagao, T. Mitamura, X. H. Wang, S. Negoro, T. Yomo, I. Urabe and H. Okada, *J Bacteriol*, 1992, **174**, 5013-5020.
48. C. E. Naylor, S. Gover, A. K. Basak, M. S. Cosgrove, H. R. Levy and M. J. Adams, *Acta Crystallographica Section D-Structural Biology*, 2001, **57**, 635-648.
49. L. F. Zhu, X. L. Xu, L. M. Wang, H. Dong, B. Yu and Y. H. Ma, *Applied and Environmental Microbiology*, 2015, **81**, 6294-6301.
50. E. Oh, F. K. Fatemi, M. Currie, J. B. Delehanty, T. Pons, A. Fragola, S. Leveque-Fort, R. Goswami, K. Susumu, A. L. Huston and I. L. Medintz, *Particle & Particle Systems Characterization*, 2013, **30**, 453-466.
51. R. Agarwal, M. S. Domowicz, N. B. Schwartz, J. Henry, I. Medintz, J. B. Delehanty, M. H. Stewart, K. Susumu, A. L. Huston, J. R. Deschamps, P. E. Dawson, V. Palomo and G. Dawson, *ACS Chemical Neuroscience*, 2015, **6**, 494-504.
52. J. C. Breger, K. Susumu, G. Lasarte-Aragones, S. A. Diaz, J. Brask and I. L. Medintz, *ACS Sensors*, 2020, **5**, 1295-1304.
53. J. B. Blanco-Canosa, M. Wu, K. Susumu, E. Petryayeva, T. L. Jennings, P. E. Dawson, W. R. Algar and I. L. Medintz, *Coordination Chemistry Reviews*, 2014, **263**, 101-137.
54. J. A. Bornhorst and J. J. Falke, *Applications of Chimeric Genes and Hybrid Proteins, Pt A*, 2000, **326**, 245-254.
55. D. E. Prasuhn, J. R. Deschamps, K. Susumu, M. H. Stewart, K. Boeneman, J. B. Blanco-Canosa, P. E. Dawson and I. L. Medintz, *Small*, 2010, **6**, 555-564.
56. L. M. Sander, *Contemporary Physics*, 2000, **41**, 203-218.
57. J. N. Vranish, M. G. Ancona, E. Oh, K. Susumu and I. L. Medintz, *Nanoscale*, 2017, **9**, 5172-5187.
58. A. Cornish-Bowden, *Fundamentals of Enzyme Kinetics, 4th ed.;*, Wiley-Blackwell, Weinheim, Germany, 2012.
59. C. W. Brown, E. Oh, D. A. Hastman, S. A. Walper, K. Susumu, M. H. Stewart, J. R. Deschamps and I. L. Medintz, *RSC Advances*, 2015, **5**, 93089-93094.
60. A. P. Malanoski, J. C. Breger, C. W. Brown, J. R. Deschamps, K. Susumu, E. Oh, G. P. Anderson, S. A. Walper and I. L. Medintz, *Nanoscale Horizons*, 2017, **2**, 241-252.
61. J. C. Breger, M. G. Ancona, S. A. Walper, E. Oh, K. Susumu, M. H. Stewart, J. R. Deschamps and I. L. Medintz, *ACS Nano*, 2015, **9**, 8491-8503.
62. J. C. Breger, S. A. Walper, E. Oh, K. Susumu, M. H. Stewart, J. R. Deschamps and I. L. Medintz, *Chemical Communications*, 2015, **51**, 6403-6406.
63. E. Maurer and G. Pfleiderer, *Z Naturforsch - Section C Journal of Biosciences*, 1987, **42**, 907-915.
64. C. M. Green, J. Spangler, K. Susumu, D. A. Stenger, I. L. Medintz and S. A. Díaz, *ACS Nano*, 2022, **16**, 20693–20704.
65. O. Idan and H. Hess, *ACS Nano*, 2013, **7**, 8658-8665.
66. Y. F. Zhang and H. Hess, *ACS Catalysis*, 2017, **7**, 6018-6027.
67. Y. F. Zhang, S. Tsitkov and H. Hess, *Nature Communications*, 2016, **7**, 13982.
68. Y. F. Zhang, Q. Wang and H. Hess, *ACS Catalysis*, 2017, **7**, 2047-2051.
69. L. Lancaster, W. Abdallah, S. Banta and I. Wheeldon, *Chemical Society Reviews*, 2018, **47**, 5177-5186.

70. J.-L. Lin, L. Palomec and I. Wheeldon, *ACS Catalysis*, 2014, **4**, 505-511.
71. J.-L. Lin and I. Wheeldon, *ACS Catalysis*, 2013, **3**, 560-564.
72. W. Abdallah, X. Hong, S. Banta and I. Wheeldon, *Current Opinion in Biotechnology*, 2022, **73**, 233-239.
73. W. P. Klein, R. P. Thomsen, K. B. Turner, S. A. Walper, J. Vranish, J. Kjems, M. G. Ancona and I. L. Medintz, *ACS Nano*, 2019, **13**, 13677-13689.
74. M. Abbas, W. P. Lipin, J. Wang and E. Spruijt, *Chemical Society Reviews*, 2021, **50**, 3690-3705.
75. A. Jain, S. Kassem, R. S. Fisher, B. R. Wang, T. D. Li, Y. He, S. Elbaum-Garfinkle, R. V. Ulijn and T. Wang, *Journal of the American Chemical Society*, 2022, **144**, 15002-15007.
76. K. E. Sapsford, K. M. Tyner, B. J. Dair, J. R. Deschamps and I. L. Medintz, *Analytical Chemistry*, 2011, **83**, 4453-4488.
77. S. L. Hooe, G. A. Ellis and I. L. Medintz, *RSC Chemical Advances*, 2022, **3**, 1301-1313.
78. G. M. Lin, R. Warden-Rothman and C. A. Voight, *Current Opinion in Systems Biology*, 2019, **14**, 82-107.
79. B. Ertek, C. Akgül and Y. Dilgin, *RSC Advances*, 2016, **6**, 20058-20066.
80. M. Riedel, W. J. Parak, A. Ruff, W. Schuhmann and F. Lisdat, *ACS Catalysis*, 2018, **8**, 5212-5220.
81. I. Shitanda, Y. Fujimura, T. Takarada, R. Suzuki, T. Aikawa, M. Itagaki and S. Tsujimura, *ACS Sensors*, 2021, **6**, 3409-3415.
82. R. Suzuki, I. Shitanda, T. Aikawa, T. Tojo, T. Kondo, S. Tsujimura, M. Itagaki and M. Yuasa, *Journal of Power Sources*, 2020, **479**, 228807.
83. S. A. Díaz, J. C. Breger and I. L. Medintz, in *Methods in Enzymology*, ed. C. V. Kumar, Academic Press, 2016, vol. 571, pp. 19-54.
84. K. E. Sapsford, D. Farrell, S. Sun, A. Rasooly, H. Mattoussi and I. L. Medintz, *Sensors and Actuators B-Chemical*, 2009, **139**, 13-21.
85. P. T. Snee, Y. H. Chan, D. G. Nocera and M. G. Bawendi, *Advanced Materials*, 2005, **17**, 1131-1136.
86. K. Susumu, L. D. Field, E. Oh, M. Hunt, J. B. Delehanty, V. Palomo, P. E. Dawson, A. L. Huston and I. L. Medintz, *Chemistry of Materials*, 2017, **29**, 7330-7344.
87. K. Susumu, B. C. Mei and H. Mattoussi, *Nature Protocols*, 2009, **4**, 424-436.
88. K. Susumu, E. Oh, J. B. Delehanty, F. Pinaud, K. B. Gemmill, S. Walper, J. Breger, M. J. Schroeder, M. H. Stewart, V. Jain, C. M. Whitaker, A. L. Huston and I. L. Medintz, *Chemistry of Materials*, 2014, **26**, 5327-5344.
89. C. M. Green, D. A. Hastman, D. Mathur, K. Susumu, E. Oh, I. L. Medintz and S. A. Diaz, *ACS Nano*, 2021, **15**, 9101-9110.
90. J. C. Claussen, W. R. Algar, N. Hildebrandt, K. Susumu, M. G. Ancona and I. L. Medintz, *Nanoscale*, 2013, **5**, 12156-12170.
91. J. C. Claussen, A. Malanoski, J. C. Breger, E. Oh, S. A. Walper, K. Susumu, R. Goswami, J. R. Deschamps and I. L. Medintz, *Journal of Physical Chemistry C*, 2015, **119**, 2208-2221.
92. J. L. Liu, D. Zabetakis, J. C. Breger, G. P. Anderson and E. R. Goldman, *Frontiers in Bioengineering and Biotechnology*, 2020, **8**, 571.
93. E. Gasteiger, A. Gattiker, C. Hoogland, I. Ivanyi, R. D. Appel and A. Bairoch, *Nucleic Acids Research*, 2003, **31**, 3784-3788.